Peremennye Zvezdy (*Variable Stars*) **45**, No. 2, 2025

Received 3 January; accepted 17 January.

DOI: 10.24412/2221-0474-2025-45-7-31

Mid-infrared Period-luminosity Relations of RR Lyrae Variables via Color-transformed Data

A. K. Dambis, L. N. Berdnikov

Sternberg Astronomical Institute, Moscow State University, Universitetskij pr. 13, Moscow 119992, Russia; leonid.berdnikov@gmail.com

We derive RR Lyrae period–metallicity–mid-infrared luminosity relations in the WISE $W1$ and $W2$ bands based on intensity-mean $W1$ and $W2$ magnitudes computed from intensity-mean Gaia G_{BP} and G_{RP} magnitudes and known metallicity [Fe/H] for $\sim$ 5000 field RR Lyrae variables and $\sim$ 700 variables in 24 globular clusters: $< M_{W1} >= -0.486(\pm0.004) - 2.418(\pm0.021)(\log P_F + 0.25) + 0.166(\pm0.007)([\mathrm{Fe/H}]+1.6)$ and $< M_{W2} >= -0.464(\pm0.004) - 2.449(\pm0.021)(\log P_F + 0.25) + 0.170(\pm0.007)([\mathrm{Fe/H}]+1.6.)$ The period slopes are based on period–magnitude relations for RR Lyraes in globular clusters and the zero points and metallicity slopes, on bias-corrected Gaia DR3 trigonometric parallaxes of field variables. The scatter of the derived relations depends on magnitude and varies from $\sim 0\overset{\mathrm{m}}{.}02$ for bright stars to $\sim 0\overset{\mathrm{m}}{.}17$ for LMC RR Lyraes. We find the period–magnitude relations for Gaia color-transformed intensity-mean $W1$- and $W2$-band magnitudes for $\sim$ 12000 LMC RR Lyraes to have practically the same slopes: $< W1_0 >= 18.039(\pm0.002) - 2.414(\pm0.020)(\log P_F + 0.25) \pm 0.166$ and $< W2_0 >= 18.061(\pm0.002) - 2.448(\pm0.020)(\log P_F + 0.25) \pm 0.168$. The distances to globular clusters implied by the derived period–metallicity–mid-infrared luminosity relations are, on the average, longer by a factor of 1.016 ± 0.010 than those inferred by Baumgardt & Vasiliev from trigonometric parallaxes of individual cluster members or totally consistent with them (a factor of 0.994 ± 0.016 or 0.992 ± 0.016) if the comparison allows for eventual parallax bias, which in that case is found to be (5.4–5.6)$\pm$ 2.8 μas in the sense that Baumgardt & Vasiliev parallaxes appear to be slightly overestimated. Our photometric distances are shorter by a factor of $\sim 1.028\pm0.010$ and $\sim 1.024\pm0.016$ than kinematical distances computed using Gaia EDR3 or Hubble Space Telescope-based proper-motion dispersion profiles, respectively.

1 Introduction

RR Lyrae variables are old low-mass pulsating core-helium-burning stars occupying the instability strip. Most of them are fundamental-mode pulsators (RRab), a smaller fraction pulsates in the first overtone (RRc), and very few of them pulsate in both modes simultaneously (RRd). RR Lyraes serve as valuable distance indicators and kinematical tracers because they obey a rather tight photometric-band-dependent period–metallicity–luminosity relations of the form:

$$< M_X >= \alpha_X \cdot \log P_F + \beta_X \cdot [\mathrm{Fe/H}] + \gamma_X \quad (1)$$

(Catelan et al. 2004). Here $< M_X >$ is the intensity-mean absolute magnitude in the photometric band X and P_F is the fundamental (or, in the case of overtone pulsators, fundamentalized) period, which is equal to the variability period P for fundamental-mode pulsators (RRab) and $P_F = P/0.746$ or $\log P_F = \log P + 0.127$ (Iben 1974) for first-overtone pulsators (RRc), respectively. The V-band absolute magnitude of RR Lyrae

stars depends on metallicity and exhibits no appreciable dependence on period, whereas near- and mid-ifrared luminosities of these variables clearly depend both on period and metallicity (Marconi et al. 2015; Neeley et al. 2017). Period–metallicity–luminosity relations in the infrared are better suited for determining photometric distances to RR Lyraes for two major reasons. First, interstellar extinction is much smaller in the infrared (by a factor of ~ 10 in the K band and ~ 17 in the WISE $W1$ and Spitzer 3.5 μm bands, respectively – see Yuan et al. 2013), resulting in much smaller (and practically negligible) effect of errors in the adopted extinction values. Second, amplitudes of light variations in the infrared are smaller than at shorter wavelengths, permitting the corresponding mean magnitudes to be determined with better precision.

There have been many empirical determinations of the parameters of RR Lyrae period–metallicity–luminosity relations in the near-infrared bands (JHK) using both the Baade–Wesselink method (for relatively bright field stars) and globular-cluster variables (Fernley et al. 1987; Liu & Janes 1990; Jones et al. 1992; Frolov & Samus 1999; Sollima et al. 2006; Prudil et al. 2024). The problem with the practical application of the near-IR period–metallicity–luminosity relations for actual population studies is that the three largest-area near-infrared surveys — DENIS (Epchtein et al. 1999), 2MASS (Skrutsie et al. 2006), and VISTA Hemisphere Survey, or VHS (McMahon et al. 2013) — provide only single-epoch data for this wavelength range. The multi-epoch near-infrared survey with the most extensive sky coverage is VVV (Minniti et al. 2024), but it focusses on the Galactic bulge and a part of the southern Milky-Way disk and thus covers only 500-plus square degrees.

The situation has improved substantially in the mid-infrared range with the advent of the Spitzer (Fazio et al. 2004) and WISE (Wright et al. 2010) photometric surveys where the latter provides all-sky multi-epoch coverage and therefore should be best suited for extensive RR-Lyrae-based Galactic structure and kinematics studies. However, WISE has two important limitations. First, the angular resolution, which is equal to $6\farcs1$ and $6\farcs4$ in the WISE $W1$ and $W2$ bands, respectively (Wright et al. 2010), and restricts the use of the survey data in crowded fields such as those of most of globular clusters. Second, the limited photometric sensitivity, which at the 5σ level is equivalent to 16.6 and 15.6 Vega magnitudes for the $W1$ and $W2$ bands, respectively, with the light curves becoming quite noisy and scattered already appreciably above these limits: this factor prevents bona fide study of RR Lyrae stars in all but few of relatively nearby globular clusters. Such a study was carried out by Dambis et al. (2014), who calibrated the period–luminosity–metallicity relations in the WISE $W1$ and $W2$ bands based on WISE light curves for 360 and 275 RR Lyraes in 15 and 9 Galactic globular clusters, respectively. Spitzer survey performs better in both aspects, but it has limited sky coverage and its data have so far been used to study the period–luminosity relation in only two globular clusters: Reticulum, which is located close to the LMC (Muraveva et al. 2018), and the nearby cluster M4 (Neeley et al. 2015). Mullen et al. (2023) performed the most comprehensive calibration of RR Lyrae period–luminosity–metallicity and period–Wesenheit–metallicity relations based on WISE photometry and Gaia EDR3 parallaxes (Gaia Collaboration, 2021) of about 1000 mostly relatively bright field RR Lyraes, thus circumventing the two WISE survey limitations mentioned above. However, because their study relies of field-star parallaxes, the accuracy of the inferred period slope estimates is not as good as those obtained by Dambis et al. (2014) using WISE data for RR Lyraes in nearby globular clusters despite the rather large scatter of the period–magnitude relations in individual clusters due to crowding. Here we propose another way to circumvent the above two WISE-survey limitations using intensity-mean WISE $W1$ and $W2$ magnitude estimates computed by transforming the

intensity-mean Gaia G_{BP} and G_{RP} magnitudes. This solution takes advantage of better resolution and deeper limiting magnitude of the Gaia survey compared to WISE and therefore makes it possible to study more distant globular clusters and RR Lyraes in more crowded cluster fields (e.g., stars located closer to cluster centers).

2 Calibration formulas

Formula (1) is linear in $\log P_F$ and [Fe/H], and hence all sorts of intensity-mean absolute-magnitude differences, which are distant independent and equal to the corresponding intensity-mean color indices (like, e.g., $(< G_{BP} > - < G_{RP} >)_0$, $(< W1 > - < G_{RP} >)_0$, etc.), and linear combinations thereof also obey similar linear relations of the same form. As a consequence, the same is true for extinction-free Q indices constructed from observed colors (with coefficients chosen so as to cancel out extinction). With the Cardelli et al. (1989) and O'Donnell (1994) extinction law and assuming R_V=3.1, the extinction ratios are equal to:

$$A_{GBP}/A_V = 1.08337, A_{GRP}/A_V = 0.63439, A_{W1}/A_V = 0.05688, A_{W2}/A_V = 0.03427. \quad (2)$$

With these ratios, the extinction-free $Q(G_{RP}-W1, G_{BP}-G_{RP})$ and $Q(G_{RP}-W2, G_{BP}-G_{RP})$ indices, which are equal to

$$Q(G_{RP}-W1, G_{BP}-G_{RP}) =< G_{RP} > - < W1 > -1.286\cdot < G_{BP} > - < G_{RP} > \quad (3)$$

and

$$Q(G_{RP}-W2, G_{BP}-G_{RP}) =< G_{RP} > - < W2 > -1.337\cdot < G_{BP} > - < G_{RP} >, \quad (4)$$

respectively, should depend linearly on $\log P_F$ and [Fe/H]:

$$< G_{RP} > - < W1 > -1.286 \cdot (< G_{BP} > - < G_{RP} >) = a_1 + b_1 \cdot \log P_F + c_1 \cdot [\mathrm{Fe/H}] \quad (5)$$

and

$$< G_{RP} > - < W2 > -1.337 \cdot (< G_{BP} > - < G_{RP} >) = a_2 + b_2 \cdot \log P_F + c_2 \cdot [\mathrm{Fe/H}]. \quad (6)$$

Given an appropriate calibrating sample of RR Lyraes with known $< G_{BP} >$, $< G_{RP} >$, $< W1 >$, $< W2 >$, $\log P_F$, and [Fe/H], the coefficients a_1, b_1, c_1, a_2, b_2, and c_2 can be estimated by solving sets of equations (5) and (6) via the least-squares method. Once these coefficients are computed, the mid-infrared intensity-mean magnitudes $< W1 >$ and $< W2 >$ of an RR Lyrae type variable can be estimated from its known intensity-mean Gaia DR3 magnitudes $< G_{BP} >$ and $< G_{RP} >$, fundamental period, and [Fe/H]:

$$< W1 >=< G_{RP} > -1.286 \cdot (< G_{BP} > - < G_{RP} >) - a_1 - b_1 \cdot \log P_F - c_1 \cdot [\mathrm{Fe/H}] \quad (7)$$

and

$$< W2 >=< G_{RP} > -1.337 \cdot (< G_{BP} > - < G_{RP} >) - a_2 - b_2 \cdot \log P_F - c_2 \cdot [\mathrm{Fe/H}]. \quad (8)$$

3 Calibration sample

Our calibrating sample is based on two RR Lyrae star lists with spectroscopic metallicity estimates. One is the subset of the catalog of Liu et al. (2020) including 5206 RR Lyraes with both metallicity and metallicity error estimates derived from spectra acquired within the framework of the LAMOST (Deng et al. 2012; Liu et al. 2014) and SDSS (SEGUE)

(Yanni et al. 2009) surveys and assumed to be in the UVES high-resolution-spectroscopy-based scale (Carretta et al. 2009). The second list is the catalog of 850 RR Lyraes by Muhie et al. (2021) with metallicities based on (1) original [Fe/H] estimates determined from low-resolution spectra taken with the 11-m SALT (Southern African Large Telescope) (Buckley 2006; O'Donoghue et al. 2006) in the process of the Milky wAy Galaxy wIth SALT spectroscopy (MAGIC) project (Kniazev et al. 2019) and (2) published spectroscopic [Fe/H] determinations compiled and homogenized by Dambis et al. (2013). The metallicities in the catalog of Muhie et al. (2021) are in the old Zinn and West (1984) (ZW) scale. We use the formula from Carretta et al. (2009):

$$[\mathrm{Fe/H}]_{UVES} = 1.105 \cdot [\mathrm{Fe/H}]_{ZW} + 0.160 \tag{9}$$

to transform them to the UVES scale adopted by Liu et al. (2020). The two lists have 139 stars in common, for which we adopt the [Fe/H] values from the more homogeneous catalog of Liu et al. (2020), with the combined list containing 5717 stars. We then cross-matched this combined list with the Clementini et al. (2023) calalog of stars classified as RR Lyrae variables based on an analysis of epoch photometry provided in Gaia DR3 (Gaia Collaboration 2023) and with ALLWISE Multiepoch Photometry and NEOWISE-R Single Exposure (L1b) Source Tables to extract the $W1$- and $W2$-band light curves, and derive the corresponding intensity-mean magnitudes $< W1 >$ and $< W2 >$. We compute $< W1 >$ and $< W2 >$ by fitting Fourier series with up to seventh harmonic to the light curves containing at least 35 data points with available uncertainty estimates. We retain only stars for which all the following data are available: (1) spectroscopic [Fe/H] estimate from Liu et al. (2020) or Muhie et al. (2021); (2) both the intensity-mean Gaia magnitudes $< G_{BP} >$ and $< G_{RP} >$ together with variability periods and pulsation modes from Clementini et al. (2023), and (3) WISE $< W1 >$-band intensity mean magnitude based on at least 35 individual photometric measurements accompanied with uncertainty estimates in the combined ALLWISE Multiepoch Photometry and NEOWISE-R Single Exposure (L1b) Source Tables. The resulting sample contains a total of 4845 RR Lyrae variables, with 4010 stars having also WISE $< W2 >$-band intensity mean values based on at least 35 individual data points, accompanied with uncertainty estimates. Note, however, that, because of the photometric sensitivity limits, the quality of WISE photometry degrades already well above the limiting magnitude. This is apparent from both the dependence of the light-curve scatter (see Fig. 1) and, especially, from that of the $< W1 > - < W2 >$ magnitude difference (Fig. 2) on $< W1 >$. To reduce the effect of photometry quality degradation, we further exclude stars fainter than $< W1 >$ =14.0 from our final calibration sample, which thus contains a total of 1633 stars and all of them also have WISE $< W2 >$-band intensity mean magnitudes based on at least 35 bona fide individual photometric measurements. With this final sample, the iteratively 3σ-clipped linear least square fits of Equations (5) and (6) for 1293 fundamental- and double-mode RR Lyraes (RRab and RRd) are:

$$\begin{aligned} < G_{RP} > - < W1 > -1.286 \cdot (< G_{BP} > - < G_{RP} >) = -0.042\ (\pm\ 0.007) \\ -0.118\ (\pm\ 0.017) \cdot \log P_F - 0.031\ (\pm\ 0.002) \cdot [\mathrm{Fe/H}]\ \pm\ 0.037 \end{aligned} \tag{10}$$

and

$$\begin{aligned} < G_{RP} > - < W2 > -1.337 \cdot (< G_{BP} > - < G_{RP} >) = -0.098\ (\pm\ 0.008) \\ -0.115\ (\pm\ 0.020) \cdot \log P_F - 0.036\ (\pm\ 0.003) \cdot [\mathrm{Fe/H}]\ \pm\ 0.042. \end{aligned} \tag{11}$$

The corresponding fits for 335 first-overtone RR Lyraes (RRc) are:

$$< G_{RP} > - < W1 > -1.286 \cdot (< G_{BP} > - < G_{RP} >) = +0.008\ (\pm\ 0.018)$$

$$-0.022\ (\pm\ 0.030)\cdot\ \log P_F - 0.009\ (\pm\ 0.004)\cdot[\mathrm{Fe/H}]\ \pm\ 0.027 \tag{12}$$

and

$$< G_{RP} > - < W2 > -1.337\cdot(< G_{BP} > - < G_{RP} >) = -0.036\ (\pm\ 0.021)$$
$$-0.025\ (\pm\ 0.036)\cdot\log P_F - 0.007\ (\pm\ 0.004)\cdot[\mathrm{Fe/H}]\ \pm\ 0.034. \tag{13}$$

Equations (7)–(13) imply the following transformation formulas:

$$< W1 >= +0.042 - 1.286\cdot < G_{BP} > +2.286\cdot < G_{RP} >$$
$$+0.118\cdot\log P_F + 0.031\cdot[\mathrm{Fe/H}] \tag{14}$$

and

$$< W2 >= +0.098 - 1.337\cdot < G_{BP} > +2.337\cdot < G_{RP} >$$
$$+0.115\cdot\log P_F + 0.036\cdot[\mathrm{Fe/H}] \tag{15}$$

for RRab- and RRd-type variables and:

$$< W1 >= -0.007 - 1.286\cdot < G_{BP} > +2.286\cdot < G_{RP} >$$
$$+0.022\cdot\log P_F + 0.009\cdot[\mathrm{Fe/H}] \tag{16}$$

and

$$< W2 >= +0.036 - 1.337\cdot < G_{BP} > +2.337\cdot < G_{RP} >$$
$$+0.025\cdot\log P_F + 0.007\cdot[\mathrm{Fe/H}] \tag{17}$$

for RRc-type variables. We point out two important properties of the above formulas: (1) their rather small scatter (about $0\overset{\mathrm{m}}{.}03$–$0\overset{\mathrm{m}}{.}04$) and (2) small (for RRab-type stars) or insignificant (for RRc-type stars) "metallicity slopes", permitting the intensity-mean infrared magnitudes to be rather accurately inferred even if metallicity is poorly known or just set equal to the average value for the population considered (e.g., $< [\mathrm{Fe/H}] > \sim -1.6$ for the Galactic halo; de Jong et al. 2010).

4 Calibration of the Period–Metallicity–Luminosity relation

4.1 The period slope

We start by determining the period slopes (α_{W1} and α_{W2}) of the $W1$- and $W2$-band Period–Metallicity–Luminosity relations (equation (1)) for RR Lyrae stars using Gaia photometry-based estimates of the $< W1 >$ and $< W2 >$ intensity-means of globular-cluster RR Lyraes computed via formulas (14–17). To this end, we first cross-match the catalog of Clementini et al. (2023) with the new version of the catalog of Milky-Way globular clusters by Harris (2010) within the clusters' tidal radii. To exclude likely fore- and background RR Lyraes, we retain only stars whose V-band magnitudes are within $0\overset{\mathrm{m}}{.}5$ of the cluster horizontal-band magnutude given in the catalog. To compute the V-band magnitudes of the stars of our sample from their $< G_{BP} >$ and $< G_{RP} >$ magnitudes from the catalog of Clementini et al. (2023), we use the following formula:

$$< V >=< G_{BP} > -(0.008 \pm 0.008) - (0.158 \pm 0.012)(< G_{BP} > - < G_{RP} >) \pm 0.044,$$

derived by fitting homogenized intensity-mean V-band magnitudes from Dambis et al. (2013) combined with V-band intensity means based on CCD observations of Muhie et al. (2021). We then exclude stars whose Gaia G_{BP} and G_{RP} fluxes are likely to be affected by contamination because of the strong crowding in central parts of globular-cluster fields. We do this by excluding all stars with the corrected BP and RP flux

excess factor C^* of Riello et al. (2021) greater than $C^* = 0.1$. The C^* quantity is equal to the original BP and RP flux excess factor introduced by Evans et al. (2018) and defined as a simple ratio between the total flux in G_{BP} and G_{RP} bands, and the G-band flux, i.e., $C = (I_{BP} + I_{RP})I_G$, minus the function $f(G_{BP} - G_{RP})$ that takes into account the color dependence of C. Whereas, due to the shape of the passbands, stars with uncontaminated I_{BP} and I_{RP} fluxes have C values slightly greater than unity, their corrected C^* factors are, by construction, close to zero. The C and C^* factors of stars that appreciably suffer from crowding should be significantly greater than unity and zero, respectively, because BP and RP fluxes, I_{BP} and I_{RP}, are not deblended and are calculated as the sum of the flux in a window of 3.5×2.1 arcsec^2, whereas the G-band flux I_G is computed from LSF or PSF fitting to a narrow image (with the pixel size of 58.9 and 176.8 mas, respectively, in the along- and across-the-scan directions).

To estimate the period slope α_{W1} or α_{W2} for a particular cluster, we use the procedure employed by Dambis et al. (2014) and just slightly modify the final step. The revised procedure goes as follows. Given that stars in a cluster are located practically at the same distance and (generally) have the same metallicity and the same amount of interstellar extinction (in any case, the latter is at least 17 times smaller in all WISE passbands compared to the V band and therefore its variations can therefore be ignored), equation (1) becomes:

$$< X > -\alpha_X \ (\log P_F + 0.25) = CC_X, \tag{18}$$

where $CC_X = \beta_X$ [Fe/H] $+ \gamma_X + (m - M)_0 + A_X - 0.25\alpha_X$ can be treated as a constant. We add the $+0.25$ term to $\log P_F$ in order to center the solution at $\log P_F = -0.25$, which is close to the average value of this parameter, so that the CC_X constant would be representative of the cluster distance modulus, in order to minimize the effect of differences in the inferred α_X values between different clusters. To estimate the constant CC_X for some assumed slope α_X, we proceed as follows. We compute the left-hand side of equation (18), $CC_{\alpha,i} =< X > -\alpha_X \ (\log P_{F,i} + 0.25)$, for each star. We then sort the $CC_{\alpha,i}$ values in the ascending order and try every subset $\mu = \{j, j+1...j+N_1-1\}$ containing $N_1 = N \times q$ consecutive values with $q = 0.68$ (where N is the total number of RR Lyraes in the given cluster after all the above cuts performed) and seek the subset $\mu = \{j, j+1...j+N_1-1\}$ having the smallest dispersion of computed CC_α values, $\sigma CC_{\alpha,\mu}$. We then try α values from –1.0 to –5.0 in increments of 0.01 to find the one yielding the smallest $\sigma CC_{\alpha,\mu}$. If the modal "core" of the distribution (i.e., the part of the distribution corresponding to stars whose data points outline the $\log P_F - < X >$ relation assumed to be linear) of $CC_{\alpha,i}$ values were normal, our subset would roughly consist at least of all stars with $CC_{\alpha,j}$ between $< CC > -\sigma CC$ and $< CC > +\sigma CC$, where $< CC >$ and σCC are the mean and dispersion of CC values for the subset of stars defining the linear $\log P_F - < X >$ relation, respectively. The mean CC value averaged over the subset stars, $< C_\mu >$, should then be close to the mean $< CC >$, and the (truncated) dispersion σCC_μ should be roughly equal to $\sigma CC_{\rm subset} = 0.54\sigma CC$, implying $3\sigma CC = 5.56\sigma CC_{\rm subset}$. We therefore determine the final estimate of CC and α_X by least squares solving the equation set

$$\alpha_X \ (\log P_F + 0.25) + CC =< X >, \tag{19}$$

which is just a rewritten form of equation (18), for stars with CC values in the interval $< CC_\mu > -d_{CC}(\max) \leq CC \leq < CC_\mu > +d_{CC}(\max)$. In the original version, we set $d_{CC}(\max)$ equal to $3\sigma CC = 5.56\sigma CC_\mu$ corresponding to the 0.9973 probability for a normal distribution. However, in real cases we have to deal with rather small RR Lyrae samples, and the 0.9973-probability interval has to be estimated based on the Student's t- rather than normal distribution, and so in our revised procedure we set $d_{CC}(\max) =$

$5.56\sigma CC_{\mu} \times ICTD(n_{\rm degrees\,of\,freedom}, 0.9973)/3$, where $ICTD(n_{\rm degrees\,of\,freedom}, {\rm prob})$ is the inverse Student's cumulative distribution. Hence, in our new version, stars are selected from a broader interval (whose halfwidth is equal to $d_{CC}(\max) = 7.58\sigma CC_{\rm subset}$ and $d_{CC}(\max) = 5.71\sigma CC_{\rm subset}$ for subsets consisting of 10 and 100 stars, respectively). Table 1 lists the solutions so obtained for 24 globular clusters with at least eight stars outlining the linear $\log P_F - < X >$ relation together with the cluster metalicities [Fe/H] and color excesses E_{B-V} adopted from the Harris (2010) catalog.

Here, like in Dambis et al. (2014), we plot the scaled computed intensity-mean $W1$ and $W2$ magnitudes ($< W1 > -CC_{W1}$ and $< W2 > -CC_{W2}$) for our calibrating clusters as a function of fundamentalized periods (Figs. (3–6). As it is evident from Table 1 and Figs. (3–6), the period–magnitude relation slopes are quite consistent among the clusters studied. Moreover, one can see from Figs. (7) and (8) that the slopes show only a marginal trend with metallicity: the corresponding linear weighted fits are:

$$\alpha_{W1} = -2.427(\pm\ 0.023) + (0.079 \pm 0.059)([{\rm Fe/H}] + 1.6) \tag{20}$$

and

$$\alpha_{W2} = -2.424(\pm\ 0.022) + (0.078 \pm 0.055)([{\rm Fe/H}] + 1.6). \tag{21}$$

The trends differ from zero by 1.4 σ, and, interestingly, they are in the sense opposite to that found by Dambis et al. (2014). We hereafter compute the combined solutions assuming the same slope for all clusters and using weights based on the scatter of individual-cluster PL solutions listed in Table 1. These combined solutions yield the slopes of $\alpha_{W1}({\rm combo}) = -2.418 \pm 0.021$ and $\alpha_{W2}({\rm combo}) = -2.449 \pm\ 0.022$ for the $W1$- and $W2$-band relations, respectively. Figs. (9) and (10) show the combined $\log P_F$ versus $< W1 > \ - CC_{W1}$ and $\log P_F$ versus $< W2 > \ - CC_{W2}$ plots for RR Lyraes passing the above filters in the 24 globular clusters of the final list. We list the CC_{W1} and CC_{W2} parameters obtained from these combined solutions in the last two columns of Table 1.

4.2 Intrinsic color calibration

To finalize our calibration of the mid-infrared period–metallicity–luminosity relations for RR Lyrae stars and to use it to compute distances to these variables, we need to be able to estimate interstellar extinction to individual stars. To this end, we now derive a calibration for the $G_{BP} - G_{RP}$ intrinsic colors of RR Lyrae variables based on the above final sample of globular-cluster stars. First, equations (2) imply the following formula for the $E_{GBP-GRP}/A_V$ color excess ratio:

$$E_{GBP-GRP}/A_V \ = (A_{GBP} - A_{GRP})/A_V = 1.08337 - 0.63439 = 0.44898.$$

Hence

$$E_{GBP-GRP} \ = 0.44898 A_V$$

or (in view of $A_V = 3.1 E_{B-V}$):

$$E_{GBP-GRP} = 1.392 E_{B-V}$$

and

$$(< G_{BP} > - < G_{RP} >)_0 \ =< G_{BP} > - < G_{RP} > -1.392 E_{B-V}. \tag{22}$$

We use formula (22) and E_{B-V} color excesses from Harris (2010) to fit a linear function of $\log P_F$ and [Fe/H] to the so computed intrinsic colors of the cluster RR Lyraes of our final sample:

$$(< G_{BP} > - < G_{RP} >)_0 \ = +0.861(\pm 0.013) + 0.999(\pm 0.026) \log P_F$$

$$+0.062(\pm0.006)[\mathrm{Fe/H}] \pm 0.052. \quad (23)$$

Given the extinction ratios (2), the total extinction in the $W1$ and $W2$ bands can then be computed as

$$A_{W1} = 0.127 \times (< G_{BP} > - < G_{RP} > -(< G_{BP} > - < G_{RP} >)_0) \quad (24)$$

and

$$A_{W1} = 0.076 \times (< G_{BP} > - < G_{RP} > -(< G_{BP} > - < G_{RP} >)_0), \quad (25)$$

respectively. The scatter of intrinsic color $(< G_{BP} > - < G_{RP} >)_0$ computed from formula (23) ($\sigma(< G_{BP} > - < G_{RP} >)_0 = 0.057$) contributes only about 0.007 and 0.004 to the error of the computed A_{W1} and A_{W2}, respectively.

4.3 The metallicity slope and zero point

To estimate the two remaining parameters of the period–metallicity–luminosity relation (1), β and γ, we cross-match our initial calibration sample of 5717 RR Lyraes having spectroscopic metallicity estimates with the Gaia DR3-based catalog of RR Lyrae-type variables by Clementini et al. (2023) and leave only stars for which the latter catalog provides both G_{BP}- and G_{RP}-band intensity-mean magnitudes. We use formulas (14)–(17) and (23)–(25) to compute the dereddened $W1$- and $W2$-band intensity-mean magnitudes of the stars considered. We make further astrometric and photometric quality cuts leaving only stars with RUWE ≤ 1.4, astrometric_excess_noise ≤ 0.2, corrected BP and RP flux excess factor $C^* \leq 0.1$. A total of 4658 stars pass these cuts.

Like Mullen et al. (2024), we determine β and γ by fitting period–metallicity–luminosity relation using the Astrometric Based Luminosity (ABL) A_{m_o}:

$$\omega 10^{0.2m_o-2} = 10^{0.2[\alpha(\log P_F+0.25)+\beta([\mathrm{Fe/H}]+1.6)+\gamma]}, \quad (26)$$

where ω is the Gaia DR3 trigonometric parallax in milliarcseconds with the parallax zero-point bias corrected as prescribed by Lindegren et al. (2021), m_o is the absorption-corrected apparent magnitude ($W1_0$ or $W2_0$), α is the period slope estimate inferred above from globular-cluster RR Lyraes, and β and γ are determined in the fit. Given the accurate globular-cluster-based estimates of the period slopes α_{W1} and α_{W2} inferred above, formula (26) for $W1$- and $W2$-band magnitudes can be rewritten as:

$$\omega 10^{0.2(W1_o+2.418(\log P_F+0.25))-2} = 10^{0.2[\beta_{W1}([\mathrm{Fe/H}]+1.6)+\gamma_{\mathrm{W1}}]} \quad (27)$$

and

$$\omega 10^{0.2(W2_o+2.449(\log P_F+0.25))-2} = 10^{0.2[\beta_{W2}([\mathrm{Fe/H}]+1.6)+\gamma_{\mathrm{W2}}]}, \quad (28)$$

respectively. Ordinary 4σ-clipped weighted regression fits (27) and (28) with Gaia DR3 parallaxes ω bias-corrected as prescribed by Lindegren et al. (2021) and with errors assumed to be only in the dependent variable and computed based on quoted Gaia DR3 parallax errors and assuming the scatter of $0\overset{\mathrm{m}}{.}05$ both in $W1_o$ and $W2_o$ about the period–metallicity–luminosity relation yield the following results:

$$\beta_{W1} = 0.153 \pm 0.007,\ \gamma_{W1} = -0.483 \pm 0.004, \quad (29)$$

and

$$\beta_{W2} = 0.156 \pm 0.007,\ \gamma_{W2} = -0.461 \pm 0.004. \quad (30)$$

The standard unit-weight error is equal to 1.20 in both cases, indicating that the quoted Gaia DR3 parallax errors appear to be slightly underestimated.

However, in our case there are also significant errors in independent variables [Fe/H], and simple regression fits produce biased results. To estimate and correct the biases introduced, we generate two sets of 400 simulated 4658-star samples with the parallax $\omega_{\rm sim}$ of each star computed using formulas (27) and (28) based on observed $\log P_F$, [Fe/H], and $W1_o$ or $W2_o$ values and with β_{W1}, $\gamma W1$, β_{W2}, and $\gamma W2$ parameters inferred above, adding simulated random noise normally distributed with zero mean and errors computed based on quoted Gaia DR3 parallax errors and $0\overset{\rm m}{.}05$ scatter in $W1_o$ or $W2_o$ magnitudes and then multiplied by 1.2. The simulated metrallicities [Fe/H] are equal to the observed ones plus random noise normally distributed with zero mean and quoted metallicity errors. We found the bias $\Delta\beta$ and $\Delta\gamma$ in the sense the estimated minus true value to be

$$\Delta\beta_{W1} = -0.0132 \pm 0.0004,\ \Delta\gamma_{W1} = +0.0027 \pm 0.0002,$$

and

$$\Delta\beta_{W2} = -0.0142 \pm 0.0004,\ \Delta\gamma_{W2} = +0.0027 \pm 0.0002,$$

implying the following bias-corrected values:

$$\beta_{W1} = 0.166 \pm 0.007,\ \gamma_{W1} = -0.486 \pm 0.004,$$

and

$$\beta_{W2} = 0.170 \pm 0.007,\ \gamma_{W2} = -0.464 \pm 0.004.$$

5 Results and validation

Thus, our final $W1$- and $W2$-band period–metallicity–luminosity relations for RR Lyrae variables are:

$$< M_{W1} >= -0.486(\pm0.004) - 2.418(\pm0.021)(\log P_F + 0.25) + 0.166(\pm0.007)([\mathrm{Fe/H}] + 1.6) \quad (31)$$

and

$$< M_{W2} >= -0.464(\pm0.004) - 2.449(\pm0.021)(\log P_F + 0.25) + 0.170(\pm0.007)([\mathrm{Fe/H}] + 1.6), \quad (32)$$

with standard errors about $0\overset{\rm m}{.}04$–$0\overset{\rm m}{.}05$. These relations are very close to those inferred by Mullen et al. (2023) based on WISE $W1$- and $W2$-band data for about 1000 bright RR Lyraes (recentered to our adopted central $\log P_F = -0.25$ and [Fe/H]=–1.6):

$$< M_{W1} >= -0.461(\pm0.008) - 2.440(\pm0.100)(\log P_F + 0.25) + 0.144(\pm0.014)([\mathrm{Fe/H}] + 1.6) \quad (33)$$

and

$$< M_{W2} >= -0.463(\pm0.009) - 2.540(\pm0.100)(\log P_F + 0.25) + 0.151(\pm0.014)([\mathrm{Fe/H}] + 1.6) \quad (34)$$

and differ by much higher accuracy of the period slopes and slightly steeper metallicity slopes. Note that our $W1$-band period–metallicity–luminosity relation is very close (both in terms of the slopes and slope errors) to the corresponding K_s-band relation derived by Bhardwaj et al. (2023) based on accurate homogeneous near-IR photometry of 954 RR Lyraes in 11 globular clusters anchored using 346 Milky Way field RR Lyraes with Gaia EDR3 parallaxes:

$$< M_{K_s} >= -0.495 - 2.370(\pm0.020)(\log P_F + 0.25) + 0.180(\pm0.010)([\mathrm{Fe/H}] + 1.6) \quad (35)$$

(we recentered it to $\log P_F = -0.25$ and [Fe/H]=–1.6 for consistency).

We use relations (31) and (32) combined with the $(< G_{BP} > - < G_{RP} >)_0$ intrinsic-color calibration (23) and extinction ratios (2) to compute the true distance moduli (DM_0(W1) and DM_0(W2)), the corresponding photometric parallaxes (ω_{W1} and ω_{W2}), and distances (D_{W1} and D_{W2}) for the 24 globular clusters of our final list, and compare them to the globular-cluster trigonometric parallaxes determined via Gaia EDR3 parallaxes and kinematic distances found from Gaia EDR3 or Hubble Space Telescope proper-motion dispersion profiles combined with radial-velocity dispersion profiles (Baumgardt & Vasiliev 2021). We summarize all these data in Table 2. Given that the errors of our globular-cluster photometric parallaxes and photometric distances are mush smaller than those of the cluster trigonometric parallaxes and kinematic distances reported by Baumgardt & Vasiliev (2021), we treat the former in the following weighted regression fits as independent variables with no errors and the latter as dependent variables with the corresponding quoted errors:

$$\omega_{EDR3} = 1.018(\pm0.011)\omega_{W1} \text{ (standard unit weight error} = 0.82), \quad (36)$$

$$\omega_{EDR3} = 1.016(\pm0.011)\omega_{W2} \text{ (standard unit weight error} = 0.82) \quad (37)$$

(24 clusters),

$$D(\text{kin})_{EDR3} = 1.027(\pm0.011)D_{W1} \text{ (standard unit weight error} = 1.01), \quad (38)$$

$$D(\text{kin})_{EDR3} = 1.029(\pm0.011)D_{W2} \text{ (standard unit weight error} = 1.03) \quad (39)$$

(12 clusters),

$$D(\text{kin})_{\text{HST}} = 1.028(\pm0.024)D_{W1} \text{ (standard unit weight error} = 2.00), \quad (40)$$

$$D(\text{kin})_{\text{HST}} = 1.028(\pm0.024)D_{W2} \text{ (standard unit weight error} = 2.04) \quad (41)$$

(5 clusters). As is evident from the above relations, the globular-cluster photometric distances based on our period–metallicity–luminosity relations are marginally consistent with the cluster parallaxes computed via Gaia EDR3 parallaxes of individual stars (in the sense that our distances are slightly longer, by a factor of ∼1.016–1.018 corresponding to ∼+0.04 in terms of the true distance modulus), but are shorter (by up to 2.5σ or a factor of 1.027–1.029 corresponding to ∼–0.06 in terms of true distance modulus) than the kinematical distances computed from Gaia EDR3 proper-motion dispersion profiles. A comparison with the kinematical distances computed via Hubble Space Telescope proper-motion dispersion profiles yields the same discrepancy factor, but with a greater error corresponding to about 1σ level.

Note that an analysis involving eventual bias in globular-cluster trigononetric parallax estimates reported by Baumgardt & Vasiliev (2021) yields:

$$\omega_{EDR3} = +5.4(\pm2.8)\mu\text{as} + 0.994(\pm0.016)\omega_{W1} \text{ (standard unit weight error} = 0.79), \quad (42)$$

and

$$\omega_{EDR3} = +5.6(\pm2.8)\mu\text{as} + 0.992(\pm0.016)\omega_{W2} \text{ (standard unit weight error} = 0.78), \quad (43)$$

(24 clusters), i.e. our photometric parallaxes of globular clusters appear to be totally consistent with estimates based on trigonometric parallaxes of individual cluster stars, and the unaccounted bias in globular-cluster parallaxes reported by Baumgardt & Vasiliev

(2021) appears to be of about $+5.5(\pm2.8)\mu$as in the sense that the said parallaxes are slightly overestimated.

We finally test our approach by applying to it to faint Gaia RR Lyrae variables. To this end, we cross-match the catalog of Clementini et al. (2023) with the list of Cusano et al. (2021) containing about 22000 RR Lyraes in the Large Magellanic Cloud having near-infrared photometry light curves from VISTA survey of the Magellanic Clouds system (VMC) and optical data from the Optical Gravitational Lensing Experiment (OGLE) IV survey and the Gaia Data Release 2 catalogue, which the authors consider to be LMC members. We leave only stars with corrected BP and RP flux excess factor $C^* \leq 0.1$ with our final list containing a total of 11901 stars for which we compute the WISE $W1$- and $W2$-band intensity-mean magnitudes $< W1 >$ and $< W2 >$ via formulas (14)–(17) above adopting me same [Fe/H]$= -1.6$ equal to the median value for LMC fundamental-mode RR Lyraes (Skowron et al. 2016). We do not use individual-star metallicity estimates from Cusano et al. (2021) because they are unavailable for a large fraction of the list and those available have errors comparable to or greater than the scatter of the values themselves. We then deredden $< W1 >$ and $< W2 >$ by substracting A_{W1}=0.487A_K and A_{W2}=0.294A_K extinction values, respectively, where K-band extinction estimates A_K are adopted from Cusano et al. (2021) and the extinction ratios are computed based on the Cardelli et al. (1989) and O'Donnell (1994) extinction law and assuming R_V=3.1. The 3-σ clipped regression fits of the period–magnitude relations $\log P_F - < W1 >_0$ and $\log P_F - < W2 >_0$ are:

$$< W1_0 >= 18.039(\pm0.002) - 2.414(\pm0.020)(\log P_F + 0.25) \pm 0.166 \qquad (44)$$

and

$$< W2_0 >= 18.061(\pm0.002) - 2.448(\pm0.020)(\log P_F + 0.25) \pm 0.168. \qquad (45)$$

Note that, despite the large scatter (which is to be expected for stars at the faint end of the Gaia catalog and located in a very crowded field), the slopes are remarkably close to the values inferred above from much brighter globular-cluster stars. Our relations (31) and (32), combined with the $(< G_{BP} > - < G_{RP} >)_0$ intrinsic-color calibration (23) and extinction ratios (2), yield the same true LMC distance modulus estimates $DM_0 = 18.525$ for both passbands, and these values are rather close to the very accurate estimate 18.477 ± 0.004 (statistical) ±0.026 (systematic) by Pietrzyński et al. (2019) based on observations of eclipsing binary systems composed of late-type stars and the calibration of the surface brightness–color relation. The statistical errors (±0.0015) are unrealistically small, and we consider a bona fide conservative error estimate to be 0.04–0.06 based on the largest discrepancy found in the case of the comparison of our photometric distances to globular clusters with the determinations based on Gaia EDR3 parallaxes of individual cluster stars and with the kinematical distances computed using Gaia EDR3 and Hubble Space Telescope proper motions – just enough to explain the departure from the very precise Pietrzyński et al. (2019) estimate.

6 Conclusions

We derived color transformations permitting the intensity-mean WISE $W1$- and $W2$-band magnitudes of RR Lyrae-type variables to be computed with errors $\sim 0\overset{\mathrm{m}}{.}03$ from their known Gaia DR3 intensity-mean ($< G_{BP} >$ and $< G_{RP} >$) magnitudes, fundamental periods, and [Fe/H]. We used our calibrations to study the mid-infrared fundamental period–magnitude relations in 24 Galactic globular clusters and find the average $\log P_F$ slopes to

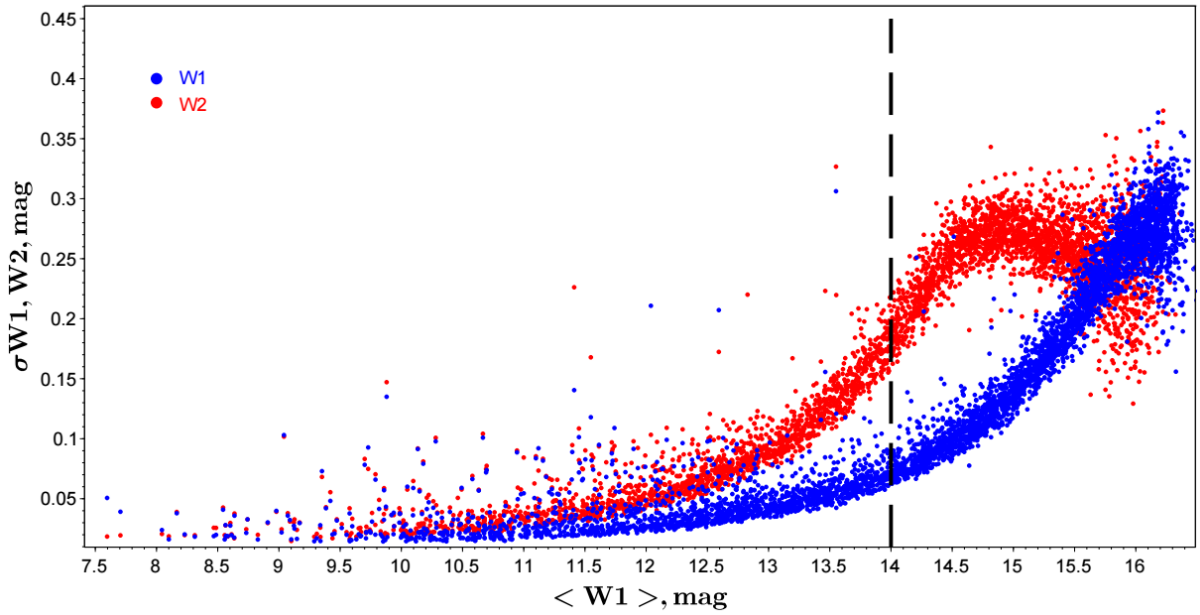

Figure 1: The rms scatter of the W1 (blue fots) and W2 (red dots) data points about the light curve as a function of $< W1 >$. The vertical dashed line at $< W1 > = 14.0$ shows the cutoff limit that we adopt to exclude stars with large scatter of mid-infrared light curves and large systematic errors (see Fig. 2 below).

be $\alpha_{W1} = -2.42 \pm 0.02$ and $\alpha_{W2} = -2.45 \pm 0.02$ for the $W1$ and $W2$ bands, respectively, and the scatter of the relations to range from $0\overset{\text{m}}{.}017$ for M 107 to $0\overset{\text{m}}{.}1$ for NGC 5824. These slope estimates, together with low-resolution spectroscopic [Fe/H] estimates for ∼5000 RR Lyraes adopted from the catalog of Liu et al. (2020) and the catalog of Muhie et al. (2021), combined with Gaia DR3 parallax and photometry data yield $W1$- and $W2$-band period–metallicity–luminosity relations with metallicity slopes β_{W1}=+0.166±0.007 and β_{W2}=+0.170±0.007, respectively. The photometric distance estimates for 24 Galactic globular clusters implied by these relations are totally consistent with average Gaia DR3 trigonometric parallaxes (with a possible parallax bias of $\sim 5.5 \pm 2.8$ μas) and about a factor of 1.028 shorter than kinematical distances computed with Gaia DR3 or HST-based proper motions. We find the $W1$- and $W2$-band fundamental period–magnitude relations for LMC RR Lyraes to have the same slopes $\alpha_{W1} = -2.42 \pm 0.02$ and $\alpha_{W2} = -2.45 \pm 0.02$ as we find for Globular-cluster variables, but much greater scatter of $\sim 0\overset{\text{m}}{.}17$. Both our $W1$- and $W2$-band period–metallicity–luminosity relations yield LMC RR Lyraes true distance modulus estimates with the mean $DM_0 = 18.53$ and a scatter of $\sigma DM_0 = 0.17$ (formal error of the mean is about 0.0015, but the actual error is determined by the zero point errors of the PML relations, transformation equations, and extinction values and may be as high as our conservative estimate of 0.06). This result is about ~ 0.06 greater than the currently best estimate 18.477 ± 0.004 (statistical) ±0.026 (systematic) obtained by Pietrzyński et al. (2019) based on LMC eclipsing variables.

7 Acknowledgments

The study was conducted under the state assignment of Lomonosov Moscow State University.

This work has made use of data from the European Space Agency (ESA) mission Gaia

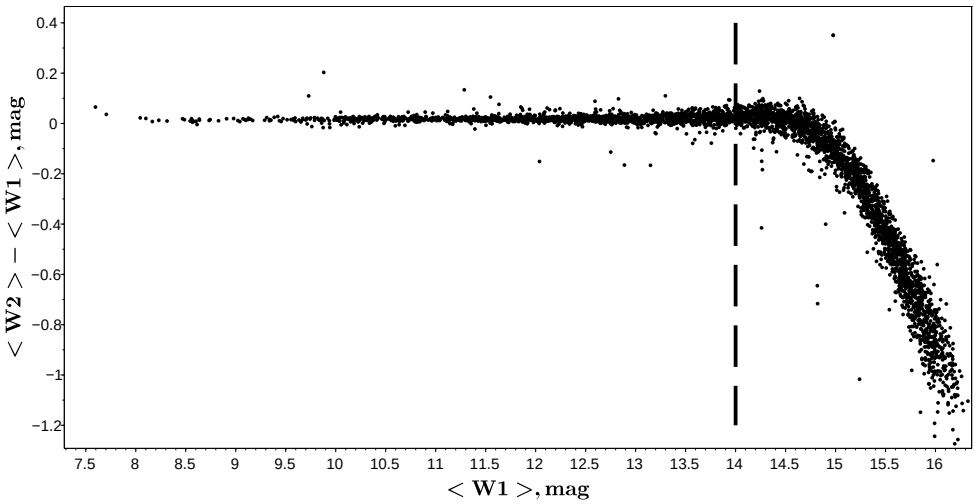

Figure 2: The $< W1 > - < W2 >$ intensity-mean magnitude difference as a function of $< W1 >$. Note that the $< W1 > - < W2 >$ difference remains practically constant up to $< W1 >$ =14.0–14.5 and then sharply decreases to about –1.1. The vertical dashed line at $< W1 >= 14.0$ shows the adopted cutoff limit used to exclude stars with large systematic errors.

(`https://www.cosmos.esa.int/gaia`), processed by the Gaia Data Processing and Analysis Consortium (DPAC, `https://www.cosmos.esa.int/web/gaia/dpac/consortium`). Funding for the DPAC has been provided by national institutions, in particular the institutions participating in the Gaia Multilateral Agreement.

This publication makes use of data products from the Wide-field Infrared Survey Explorer, which is a joint project of the University of California, Los Angeles, and the Jet Propulsion Laboratory/California Institute of Technology, funded by the National Aeronautics and Space Administration.

This publication also makes use of data products from NEOWISE, which is a project of the Jet Propulsion Laboratory/California Institute of Technology, funded by the Planetary Science Division of the National Aeronautics and Space Administration.

References:

Baumgardt, H. & Vasiliev, E. 2021, *Monthly Notices Roy. Astron. Soc.*, **505**, No. 4, 5957

Bhardwaj, A., Marconi, M., Rejkuba, M., et al. 2023, *Astrophys. J. Lett.*, **944**, No. 2, L51

Bono, G., Caputo, F., Castellani, V., et al. 2003, *Monthly Notices Roy. Astron. Soc.*, **344**, No. 4, 1097

Buckley, D. A. H., Swart, G. P., Meiring, J. G., 2006, *Proceedings of the SPIE*, **6267**, 62670Z

Butler, D. J. 2003, *Astron. & Astrophys.*, **405**, No. 3, 981

Cardelli. J. A., Clayton, G. C., & Mathis J. S. 1989,*Astrophys. J.*, **345**, No. 1, 245

Carretta, E., Bragaglia, A., Gratton, R., et al. 2009, *Astron. & Astrophys.*, **508**, No. 2, 695

Cassisi, S., Castellani, M., Caputo, F., & Castellani, V. 2004, *Astron. & Astrophys.*, **426**, No. 2, 641

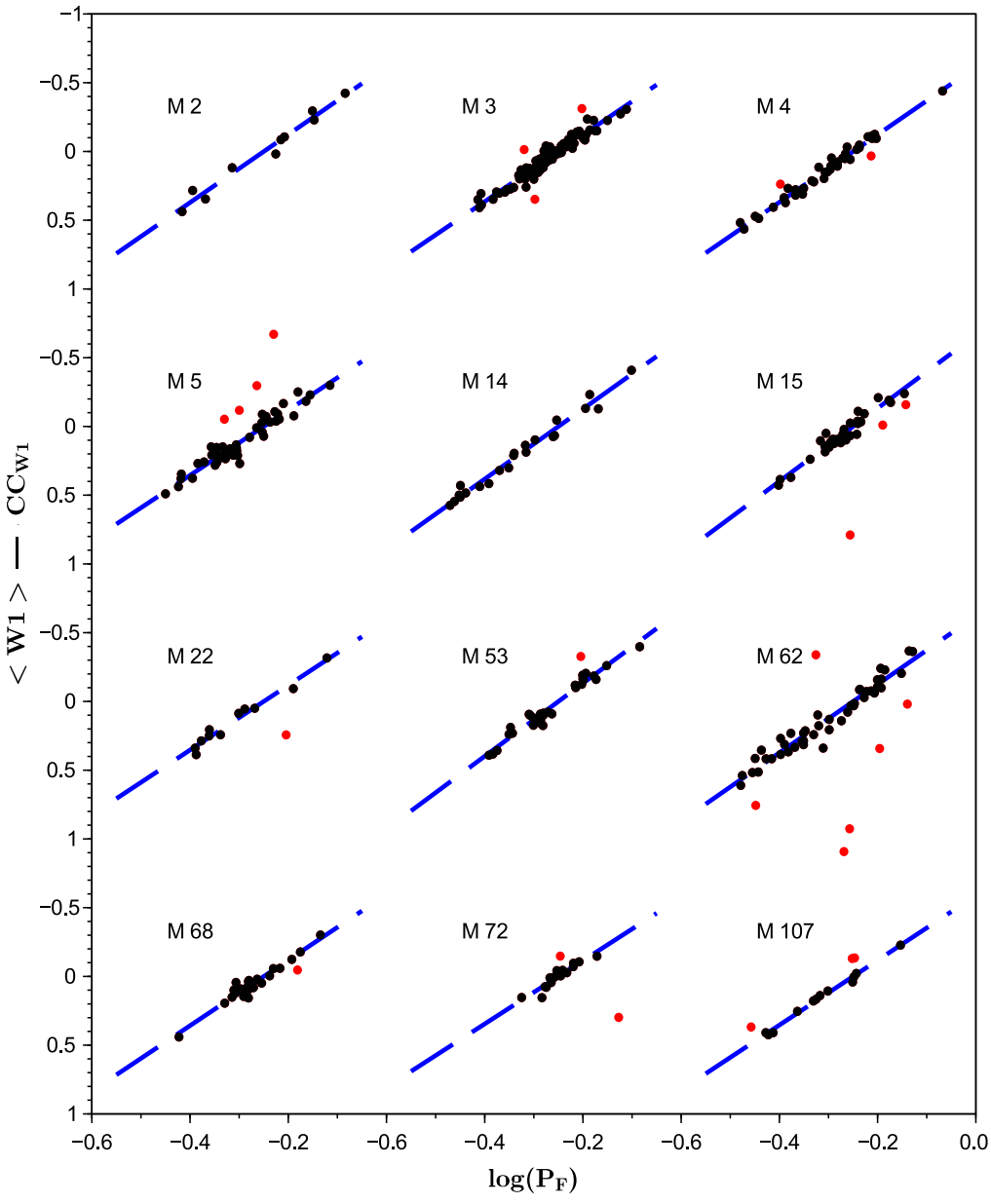

Figure 3: The PL–(transformed $W1$) relation for the RR Lyrae type variables in globular clusters M 2–M 107. The blue dashed lines show the linear fits, the black and red dots, the fitting stars and outliers, respectively. The transformed $W1$ magnitudes are scaled to the same distance, extinction, and metallicity by subtracting the parameter $CW1$ for each cluster.

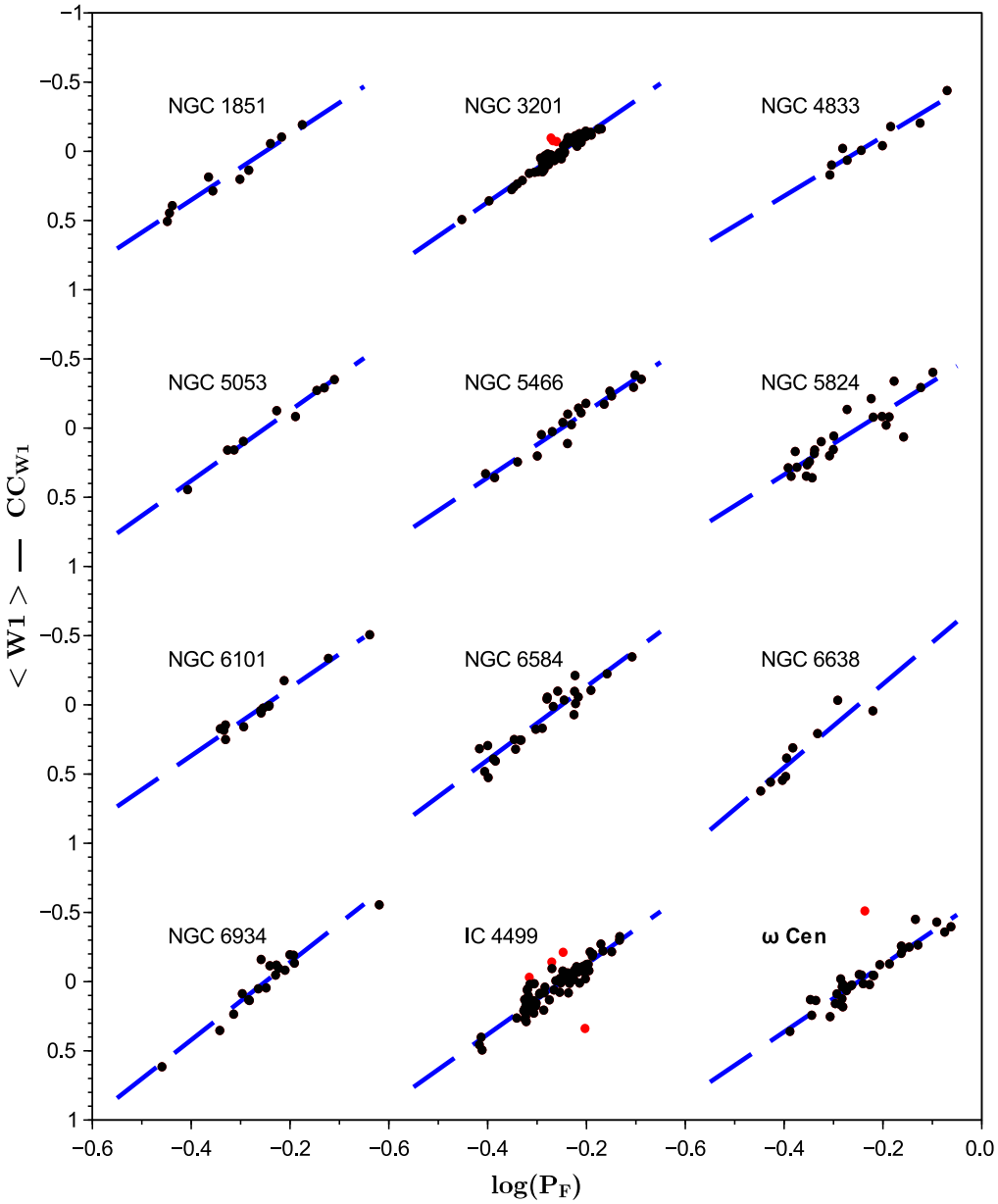

Figure 4: Same as in Fig. 3 but for the globular clusters NGC 1851–ω Cen.

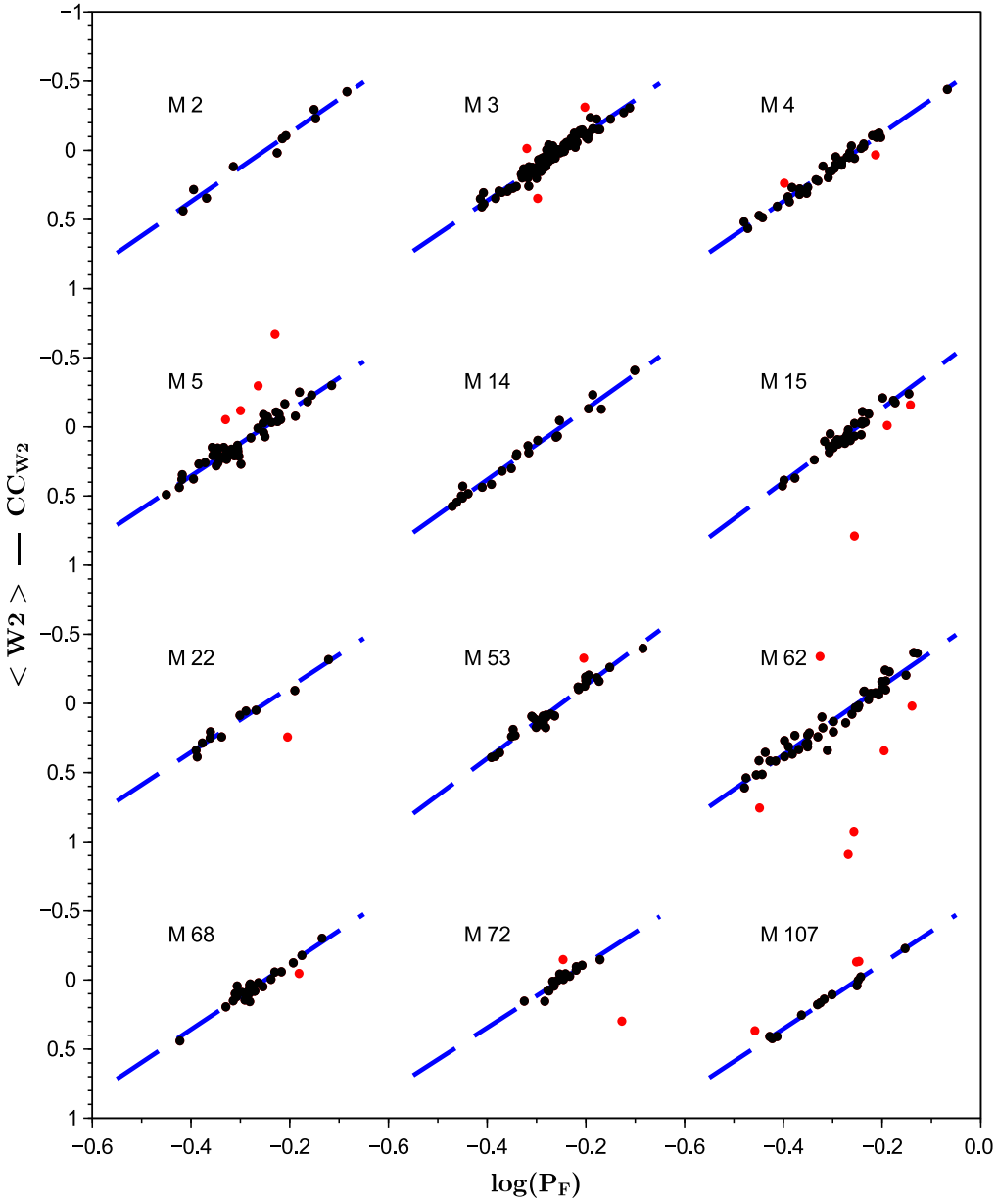

Figure 5: The PL–(transformed $W2$) relation for the RR Lyrae type variables in globular clusters M 2–M 107. The transformed $W2$ magnitudes are scaled to the same distance, extinction, and metallicity by subtracting the parameter $CW2$ for each cluster.

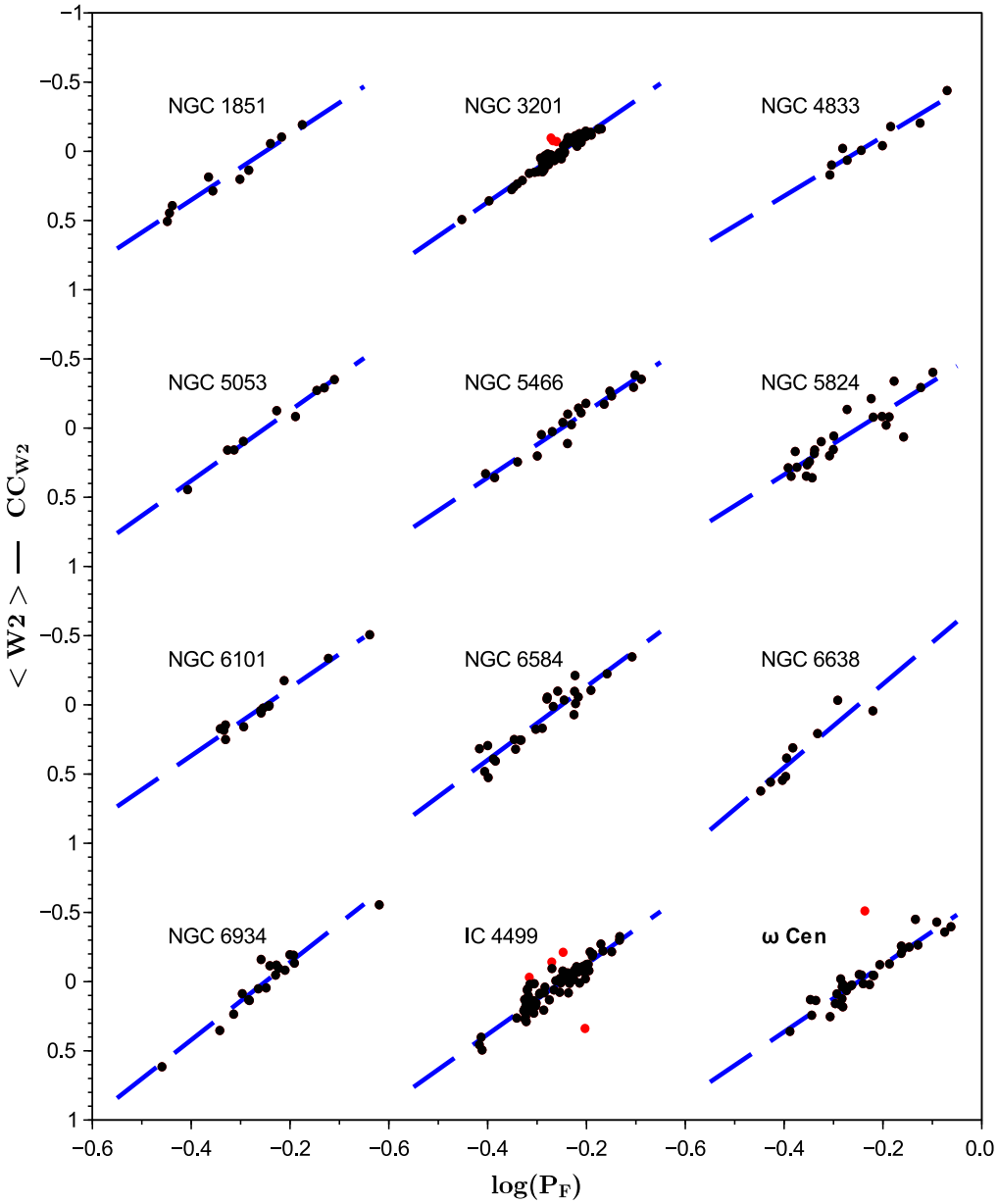

Figure 6: Same as Fig. 5 but for the globular clusters NGC 1851–ω Cen.

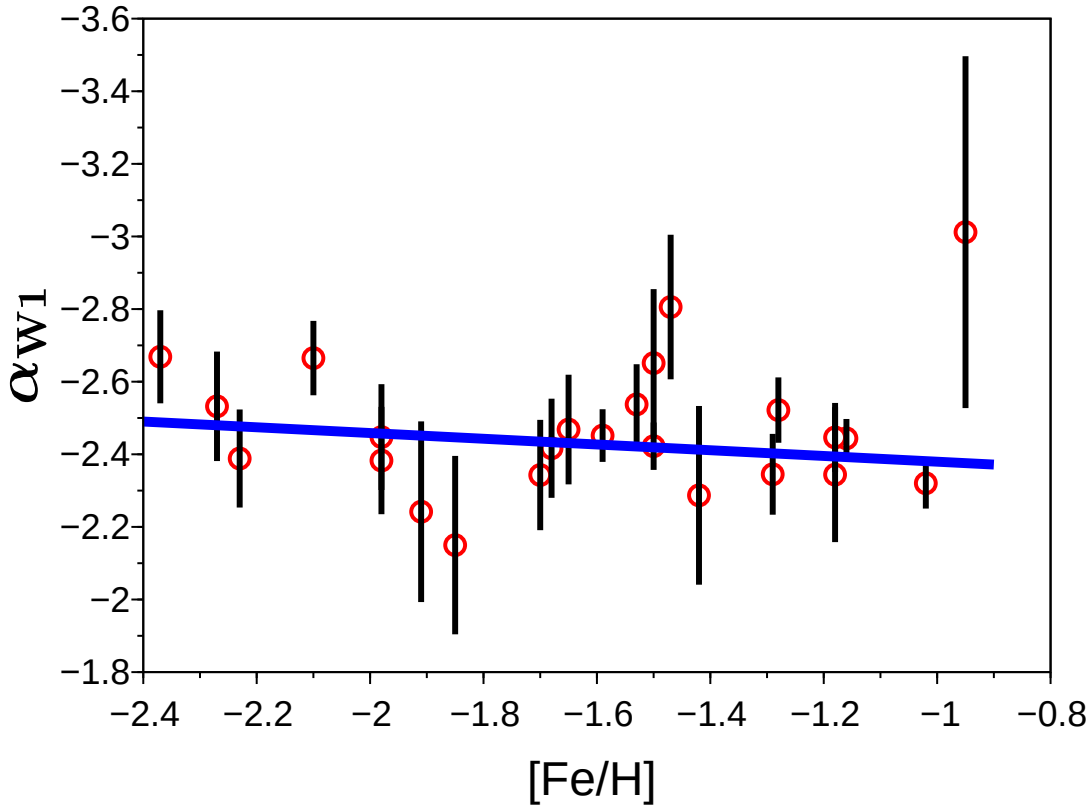

Figure 7: The period slope α_{W1} for RR Lyraes as a function of the cluster metallicity. The solid blue line shows the linear fit defined by equation (20).

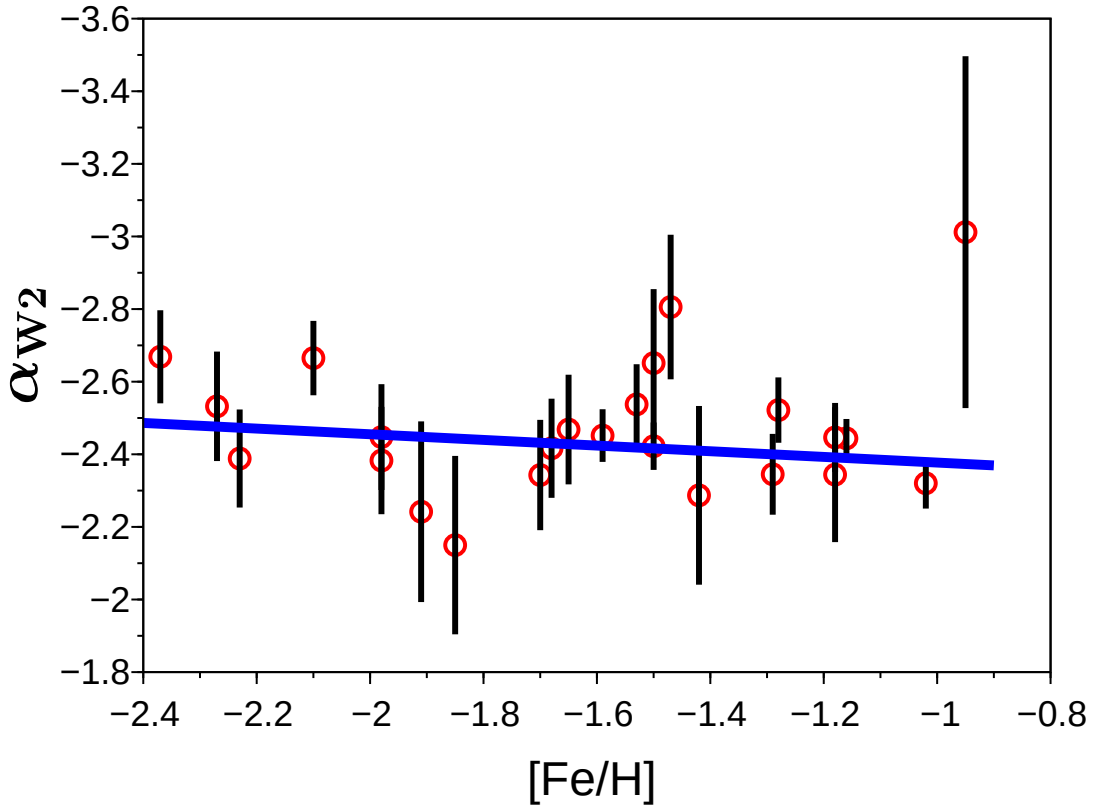

Figure 8: The period slope α_{W2} for RR Lyraes as a function of the cluster metallicity. The solid blue line shows the linear fit defined by equation (21).

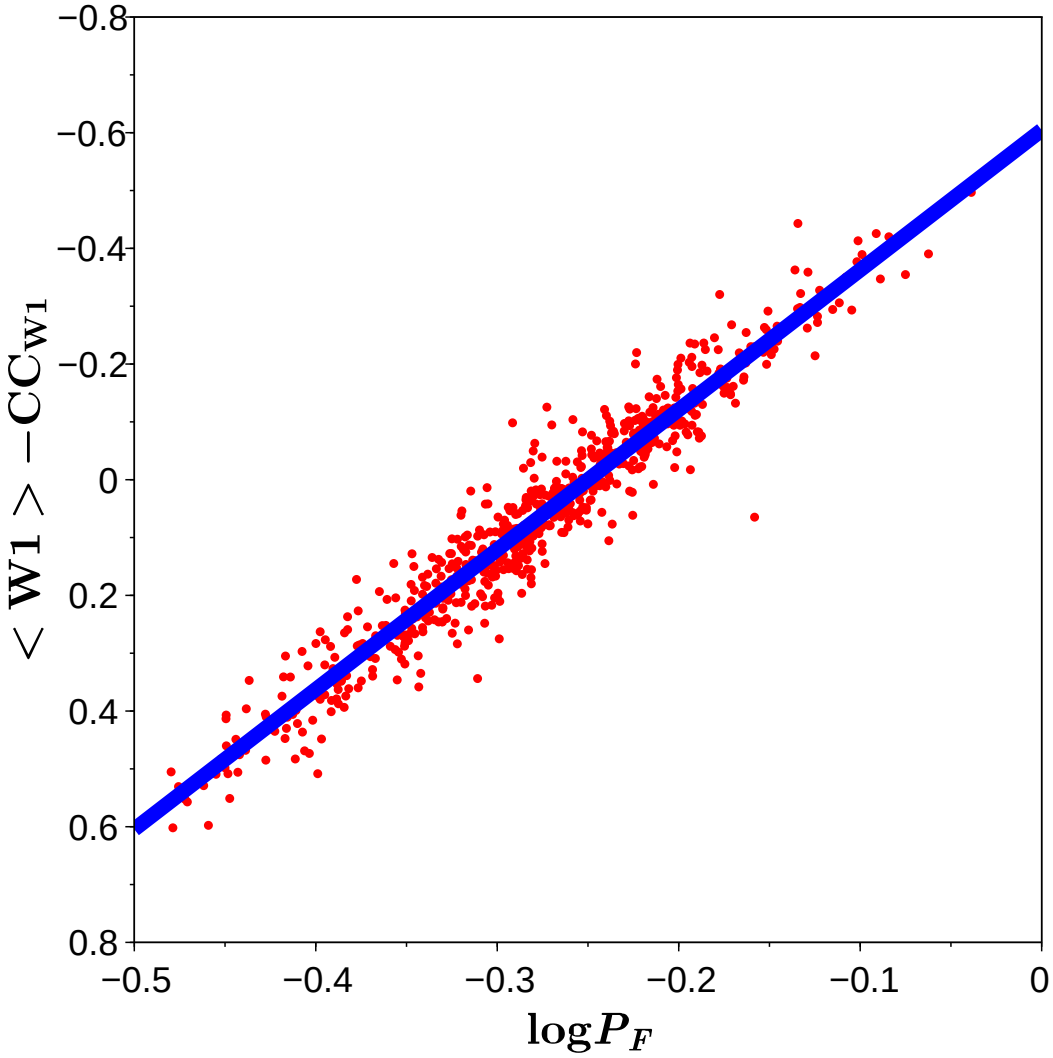

Figure 9: The combined period–$W1$-magnitude relation for our globular-cluster RR Lyrae sample. The blue line shows the resulting linear fit with $\alpha_{W1}(\mathrm{combo}) = -2.418 \pm 0.021$.

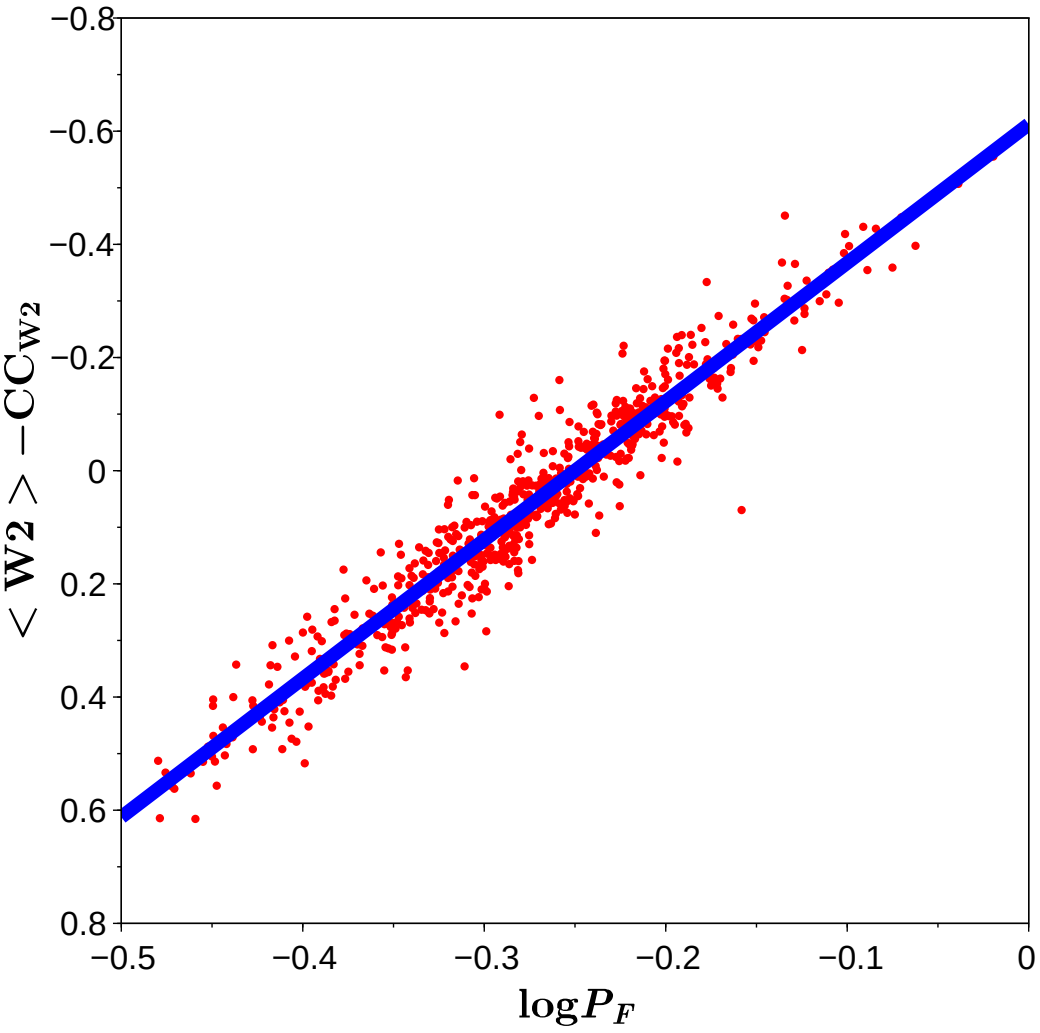

Figure 10: The combined period–$W2$-magnitude relation for our globuar-cluster RR Lyrae sample. The blue line shows the resulting linear fit with $\alpha_{W2}(\mathrm{combo}) = -2.449 \pm 0.022$.

Catelan, M., Pritzl, B. J., & Smith, H. A. 2004, *Astrophys. J., Suppl. Ser.*, **154**, No. 2, 633
Clementini, G., Ripepi, V., Garofalo, A., et al. 2023, *Astron. & Astrophys.*, **674**, article id. A18
Cusano, F., Moretti, M. I., Clementini, G., et al. 2021, *Monthly Notices Roy. Astron. Soc.*, **504**, No. 1, 1
Dambis, A., Berdnikov, L., Kniazev, A. Y., et al. 2013, *Monthly Notices Roy. Astron. Soc.*, **435**, No. 4, 3206
Dambis, A. K., Rastorguev, A. S., & Zabolotskikh, M. V. 2014, *Monthly Notices Roy. Astron. Soc.*, **439**, No. 4, 3765
Deng, L.-C., Newberg, H. J., Liu, C., et al., 2012, *Res. Astron. Astrophys.*, **12**, No. 7, 735
de Jong, J. T. A., Yanny, B., Rix, H.-W., et al. 2010, *Astrophys. J.*, **714**, No. 1, 663
Epchtein, N., Deul, E., Derriere, S., et al. 1999, *Astron. & Astrophys.*, **349**, No. 1, 236
Evans, D. W., Riello, M., De Angeli, F., et al. 2018, *Astron. & Astrophys.*, **616**, article id. A4
Fazio, G. G., Hora, J. L., Allen, L. E., et al. 2004, *Astrophys. J., Suppl. Ser.*, **154**, No. 1, 10
Fernley, J. A., Longmore, A. J., & Jameson, R. F. 1987, *Lecture Notes in Physics*, **274**, 239
Frolov, M. S. & Samus, N. N., 1998, *Astron. Lett.*, **24**, No. 2. 171
Gaia Collaboration, Prusti, T., de Bruijne, J. H. L., Brown, A. G. A., et al. 2016, *Astron. & Astrophys.*, **595**, article id. A1
Gaia Collaboration, Brown, A. G. A., Vallenari, A., Prusti, T., et al. 2021, *Astron. & Astrophys.*, **649**, article id. A1
Gaia Collaboration, Brown, A. G. A., Vallenari, A., Prusti, T., et al. 2021, *Astron. & Astrophys.*, **649**, article id. A1
Gaia Collaboration, Vallenari, A., Brown, A. G. A., Prusti, T. et al. 2023, *Astron. & Astrophys.*, **674**, article id. A1
Harris, W. E. 2010, arXiv:1012.3224
Iben Jr., I. 1974, *Ann. Rev. Astron. & Astrophys.*, 12, 215
Jones, R. V., Carney, B. W., Storm, J., & Latham, D. W. 1992, *Astrophys. J.*, **386**, No. 2, 646
Kniazev, A. Y., Usenko, I. A., Kovtyukh, V. V., & Berdnikov, L. N. 2019, *Astrophys. Bull.*, **74**, No. 2, 208
Lindegren, L., Bastian, U., Biermann, M., et al. 2021, *Astron. & Astrophys.*, **649**, article id. A4
Liu, T. & Janes, K. A., 1990, *Astrophys. J.*, **354**, No. 1, 273
Liu, X.-W., Yuan, H.-B., Huo, Z.-Y., et al. 2014, *IAUS*, **298**, 310
Liu, G.-C., Huang, Y., Zhang, H.-W., et al. 2020, *Astrophys. J., Suppl. Ser.*, **247**, article id. 68
Marconi, M., Coppola, G., Bono, G., et al. 2015, *Astrophys. J.*, **808**, No. 1, article id. 50
McMahon, R. G., Banerji, M., Gonzalez, E., et al. 2013, *Messenger*, **154**, 35
Minniti, D., Lucas, P. W., Emerson, J. P., et al. 2010, *New Astron.*, 15, 433
Muhie T. D., Dambis A. K., Berdnikov L. N., et al. 2021, *Monthly Notices Roy. Astron. Soc.*, **502**, No. 3, 4074
Mullen, J. P., Marengo, M., Martínez-Vázquez, C. E., et al. 2023, *Astrophys. J.*, **945**, No. 1, article id. 83

Muraveva, T., Garofalo, A., Scowcroft, V., et al. 2018, *Monthly Notices Roy. Astron. Soc.*, **480**, No. 3, 4138
Neeley, J. R., Marengo, M., Bono, G., et al. 2015, *Astrophys. J.*, **808**, No. 1, article id. 11
Neeley, J. R., Marengo, M., Bono, G. et al. 2017, *Astrophys. J.*, **841**, No. 2, article id. 84
O'Donoghue, D., Buckley, D. A. H., Balona, L. A., et al. 2006, *Monthly Notices Roy. Astron. Soc.*, **372**, No. 1, 151
O'Donnell, J. E. 1994, *Astrophys. J.*, **422**, No. 1, 158
Pietrzyński, G., Graczyk, D., Gallenne, A., et al. 2019, *Nature*, **567**, No. 7747, 200
Riello, M., De Angeli, F., Evans, D. W., et al. 2021, *Astron. & Astrophys.*, **649**, article id. A3
Skowron, D. M., Soszyński, I., Udalski, A., et al. 2016, *Acta Astron.*, **66**, No. 3, 269
Skrutskie, M. F., Cutri, R. M., Stiening, R., et al. 2006, *Astron. J.*, **131**, No. 2, 1163
Sollima, A., Cacciari, C., & Valenti, E. 2006, *Monthly Notices Roy. Astron. Soc.*, **372**, No. 3, 1675
Wright, E. L., Eisenhardt, P. R. M., Mainzer, A. K., et al. 2010, *Astron. J.*, **140**, No. 6, 1868
Yanny, B., Rockosi, C., Newberg, H. J., et al. 2009, *Astron. J.,* **137**, No. 5, 4377
Yuan, H. B., Liu, X. W., & Xiang, M. S. 2013, *Monthly Notices Roy. Astron. Soc.*, **430**, No. 3, 2188
Zinn, R. & West, M. J., 1984, *Astrophys. J., Suppl. Ser.*, **55**, No. 1, 45

Table 1. Parameters of the $W1 = \alpha_{W1}(\log P_F + 0.25) + CC_{W1}$ and $W2 = \alpha_{W2}(\log P_F + 0.25) + CC_{W2}$ fits for globular clusters with at least eight RR Lyraes outlining linear relation

Cluster name	Alt. name	E_{B-V}	[Fe/H]	N	CC_{W1}	α_{W1}	σ_{W1}	CC_{W2}	α_{W2}	σ_{W12}	CC_{W1} (α_{W1}= –2.418)	CC_{W2} (α_{W2}= –2.449)
NGC 7089	M 2	0.06	–1.65	10	14.804	–2.431	0.048	14.824	–2.468	0.040	14.804	14.824
					± 0.017	± 0.149		± 0.017	± 0.152		± 0.015	± 0.016
NGC 5272	M 3	0.01	–1.50	93	14.485	–2.386	0.037	14.506	–2.422	0.038	14.484	14.505
					± 0.005	± 0.064		± 0.005	± 0.066		± 0.004	± 0.004
NGC 6121	M 4	0.35	–1.16	43	10.959	–2.412	0.029	10.953	–2.443	0.029	10.959	10.952
					± 0.006	± 0.054		± 0.006	± 0.054		± 0.005	± 0.005
NGC 5904	M 5	0.03	–1.29	44	13.822	–2.321	0.054	13.843	–2.344	0.056	13.817	13.838
					± 0.010	± 0.107		± 0.010	± 0.112		± 0.008	± 0.009
NGC 6402	M 14	0.60	–1.28	22	14.343	–2.502	0.041	14.325	–2.521	0.043	14.349	14.331
					± 0.012	± 0.087		± 0.012	± 0.091		± 0.009	± 0.009
NGC 7078	M 15	0.10	–2.37	34	14.469	–2.601	0.040	14.483	–2.668	0.041	14.473	14.488
					± 0.008	± 0.125		± 0.008	± 0.129		± 0.007	± 0.007
NGC 6656	M 22	0.34	–1.70	11	12.095	–2.313	0.037	12.093	–2.342	0.040	12.088	12.087
					± 0.015	± 0.144		± 0.016	± 0.152		± 0.011	± 0.012
NGC 5024	M 53	0.02	–2.10	30	15.766	–2.604	0.039	15.787	–2.665	0.041	15.768	15.789
					± 0.008	± 0.100		± 0.008	± 0.103		± 0.007	± 0.007
NGC 6266	M 62	0.47	–1.18	46	13.496	–2.439	0.060	13.484	–2.446	0.062	13.493	13.479
					± 0.011	± 0.092		± 0.011	± 0.096		± 0.009	± 0.009
NGC 4590	M 68	0.05	–2.23	26	14.414	–2.330	0.035	14.431	–2.388	0.036	14.412	14.430
					± 0.008	± 0.133		± 0.008	± 0.136		± 0.007	± 0.007
NGC 6981	M 72	0.05	–1.42	15	15.601	–2.267	0.031	15.621	–2.286	0.033	15.601	15.620
					± 0.009	± 0.236		± 0.009	± 0.247		± 0.008	± 0.009
NGC 6171	M 107	0.33	–1.02	12	13.258	–2.305	0.017	13.253	–2.320	0.018	13.250	13.244
					± 0.007	± 0.067		± 0.008	± 0.070		± 0.005	± 0.006
NGC 1851		0.02	–1.18	10	14.855	–2.325	0.050	14.876	–2.343	0.052	14.848	14.867
					± 0.022	± 0.180		± 0.023	± 0.186		± 0.016	± 0.017
NGC 3201		0.24	–1.59	67	12.834	–2.405	0.028	12.838	–2.451	0.030	12.834	12.837
					± 0.004	± 0.069		± 0.004	± 0.073		± 0.003	± 0.004
NGC 4833		0.32	–1.85	9	13.492	–2.127	0.053	13.492	–2.149	0.054	13.500	13.500
					± 0.021	± 0.241		± 0.021	± 0.246		± 0.018	± 0.018
NGC 5053		0.01	–2.27	9	15.567	–2.476	0.040	15.588	–2.532	0.041	15.566	15.587
					± 0.015	± 0.148		± 0.015	± 0.151		± 0.014	± 0.014
NGC 5466		0.00	–1.98	19	15.391	–2.339	0.054	15.412	–2.382	0.055	15.392	15.413
					± 0.014	± 0.144		± 0.014	± 0.148		± 0.012	± 0.013
NGC 5824		0.13	–1.91	24	16.991	–2.200	0.101	17.004	–2.241	0.104	16.984	16.997
					± 0.023	± 0.241		± 0.023	± 0.249		± 0.021	± 0.022
NGC 6101		0.05	–1.98	13	15.162	–2.396	0.042	15.177	–2.447	0.043	15.161	15.177
					± 0.013	± 0.144		± 0.013	± 0.146		± 0.012	± 0.012
NGC 6584		0.10	–1.50	25	15.089	–2.617	0.081	15.104	–2.651	0.082	15.097	15.112
					± 0.019	± 0.201		± 0.019	± 0.204		± 0.016	± 0.017
NGC 6638		0.41	–0.95	9	14.385	–2.983	0.092	14.377	–3.011	0.093	14.450	14.442
					± 0.065	± 0.482		± 0.066	± 0.485		± 0.031	± 0.031
NGC 6934		0.10	–1.47	17	15.426	–2.782	0.050	15.431	–2.805	0.069	15.425	15.431
					± 0.013	± 0.146		± 0.017	± 0.200		± 0.012	± 0.016
IC 4499		0.23	–1.53	72	15.888	–2.500	0.057	15.894	–2.537	0.058	15.889	15.895
					± 0.008	± 0.108		± 0.008	± 0.111		± 0.007	± 0.007
NGC 5139	ω Cen	0.12	–1.68*	33	13.140	–2.371	0.061	13.158	–2.416	0.062	13.140	13.153
					± 0.011	± 0.135		± 0.008	± 0.137		± 0.011	± 0.011

* Because of the metallicity spread among RR Lyrae stars in this cluster (Sollima et al. 2006 and reference therein), we left only the metal-poor stars ($[Fe/H]_{\rm Zinn\&West} < -1.4$ corresponding to $[Fe/H]_{\rm Caretta} < -1.387$).

Table 2. Comparison of our RR Lyrae-based photometric distance estimates to 24 globular clusters with Gaia DR3-based trogonometric parallax estimates and Gaia DR3- and HST-based kinematical distance estimates from Vasiliev & Baumgardt (2021)

Cluster name	Alt. name	DM_0 (W1)	D_{W1}, kpc	ω_{W1}, mas	DM_0 (W2)	D_{W2}, kpc	ω_{W2}, μas	ω_{EDR3}, μas	$D_{\rm kin}$(EDR3), kpc	$D_{\rm kin}$(HST), kpc
NGC 7089	M 2	15.288	11.416	87.64	15.290	11.429	87.50	82	11.940	
		±0.016	±0.083	±0.64	±0.016	±0.085	±0.64	±11	±0.703	
NGC 5272	M 3	14.951	9.778	102.27	14.951	9.778	102.27	110	10.116	
		±0.006	±0.025	±0.26	±0.006	±0.025	±0.27	±10	±0.384	
NGC 6121	M 4	11.310	1.828	547.04	11.304	1.823	548.57	556	1.878	
		±0.006	±0.005	±1.53	±0.006	±0.005	±1.51	±10	±0.033	
NGC 5904	M 5	14.246	7.067	141.50	14.246	7.065	141.53	141	7.467	7.456
		±0.009	±0.030	±0.59	±0.009	±0.031	±0.61	±10	±0.357	±0.201
NGC 6402	M 14	14.676	8.616	116.06	14.677	8.617	116.06	129		
		±0.010	±0.040	±0.53	±0.010	±0.041	±0.54	±11		
NGC 7078	M 15	15.069	10.322	96.88	15.072	10.337	96.73	97		10.375
		±0.008	±0.038	±0.35	±0.008	±0.039	±0.36	±10		±0.295
NGC 6656	M 22	12.531	3.207	311.78	12.532	3.209	311.65	306	3.181	3.161
		±0.012	±0.018	±1.73	±0.013	±0.019	±1.81	±10	±0.123	±0.088
NGC 5024	M 53	16.333	18.475	54.13	16.336	18.504	54.04	67	17.313	
		±0.008	±0.071	±0.21	±0.008	±0.072	±0.21	±11	±1.353	
NGC 6266	M 62	13.826	5.824	171.70	13.822	5.812	172.04	185	6.395	6.502
		±0.010	±0.027	±0.78	±0.010	±0.027	±0.81	±11	±0.327	±0.163
NGC 4590	M 68	14.994	9.970	100.30	14.995	9.979	100.02	113		
		±0.008	±0.037	±0.37	±0.008	±0.038	±0.38	±11		
NGC 6981	M 72	16.048	16.203	61.72	16.048	16.207	61.70	84		
		±0.009	±0.068	±0.26	±0.009	±0.070	±0.27	±12		
NGC 6171	M 107	13.581	5.203	192.20	13.574	5.187	192.79	194	6.017	
		±0.007	±0.016	±0.58	±0.007	±0.016	±0.61	±11	±0.407	
NGC 1851		15.260	11.273	88.70	15.258	11.260	88.81	88		
		±0.017	±0.087	±0.67	±0.017	±0.089	±0.70	±11		
NGC 3201		13.276	4.520	221.24	13.274	4.517	221.37	222	4.745	
		±0.005	±0.011	±0.54	±0.005	±0.011	±0.55	±10	±0.176	
NGC 4833		13.971	6.226	160.62	13.972	6.230	160.52	164	5.822	
		±0.018	±0.053	±1.33	±0.019	±0.053	±1.36	±11	±0.360	
NGC 5053		16.161	17.071	58.58	16.163	17.088	58.52	50		
		±0.014	±0.111	±0.38	±0.014	±0.113	±0.38	±11		
NGC 5466		15.941	15.427	64.82	15.942	15.430	64.81	57		
		±0.013	±0.093	±0.39	±0.013	±0.095	±0.40	±11		
NGC 5824		17.499	31.604	31.64	17.500	31.629	31.62	57		
		±0.021	±0.311	±0.31	±0.022	±0.315	±0.31	±12		
NGC 6101		15.702	13.814	72.39	15.700	13.805	72.44	84		
		±0.012	±0.079	±0.41	±0.013	±0.080	±0.42	±11		
NGC 6584		15.548	12.872	77.68	15.548	12.872	77.69	77		
		±0.017	±0.100	±0.59	±0.017	±0.101	±0.60	±11		
NGC 6638		14.756	8.936	111.90	14.752	8.920	112.10	115		
		±0.031	±0.130	±1.59	±0.032	±0.129	±1.60	±12		
NGC 6934		15.872	14.944	66.92	15.862	14.872	67.24	78	16.718	
		±0.013	±0.090	±0.40	±0.017	±0.115	±0.52	±12	±1.382	
IC 4499		16.323	18.388	54.38	16.322	18.387	54.39	54		
		±0.008	±0.067	±0.20	±0.008	±0.068	±0.20	±11		
NGC 5139	ω Cen	13.617	5.291	188.99	13.618	5.293	188.93	193	5.359	5.264
		±0.011	±0.028	±0.99	±0.012	±0.028	±1.00	±9	±0.141	±0.121